Vol. 94 (1998) ACTA PHYSICA POLONICA A No. 2

Proc. of the XXVII Intern. School on Physics of Semiconducting Compounds, Jaszowiec 1998

ULTRAFAST PHENOMENA IN II–VI SEMICONDUCTORS

H. KALT, S. WACHTER, D. LÜERSSEN AND J. HOFFMANN

Institut für Angewandte Physik, Universität Karlsruhe, 76128 Karlsruhe, Germany

We review studies on the coherent and incoherent exciton dynamics in ZnSe-based quantum wells. First, the exciton–exciton scattering parameter is determined from femtosecond four-wave mixing as a function of background exciton density generated by a prepulse. A linear increase in the excitonic homogeneous linewidth is found as a function of the background exciton density with significant different scattering parameters for the cases of interaction with coherent or incoherent excitons. Second, the thermalization dynamics of spectrally narrow hot-exciton distributions is investigated by time-resolved phonon sideband spectroscopy. Thermalization assisted by acoustic phonons occurs on a 100 ps timescale, which is in good agreement with model calculations in time dependent perturbation theory.

PACS numbers: 78.47.+p, 42.50.Md, 71.35.–y

1. Introduction

Low-dimensional semiconductor structures like quantum wells (QWs) based on the II–VI compound ZnSe are very attractive for ultrafast and nonlinear optical spectroscopy due to some special properties not found in III–V materials.

First, the binding energies of excitons and biexcitons are rather high. The bulk value of the excitonic Rydberg energy is nearly a factor of five larger than in GaAs. In quantum wells, a typical value of the exciton binding energy is 25 meV. Consequently, the excitonic resonances have a high oscillator strength and the excitons are rather robust towards Coulomb screening even at high optical excitation. Moreover, the heavy-hole (hh) exciton ground state is sufficiently isolated in energy from excited excitonic states for selective excitation with ultrashort (i.e. spectrally broad) laser pulses. It is thus possible to study exciton–exciton interactions in ZnSe QWs solely of $1s$ hh excitons [1]. The thermalization dynamics of $1s$ hh excitons within its dispersion parabola can be investigated starting from large center-of-mass momenta, i.e., high initial excess kinetic energies [2, 3]. Also the properties of biexcitons are accessible in more detail than in III–V quantum wells [4, 5].

Secondly, the Fröhlich coupling of excitons to LO phonons in ZnSe-based QWs is about a factor of seven larger than in GaAs structures. This feature, which can be a major drawback for the performance of optical devices, is rather welcome in the case of spectroscopy. Investigation of the phonon-sideband emission gives a direct access to the exciton population within otherwise nonradiative

states at large exciton quasimomentum. Emission of LO phonons leads to an efficient exciton formation and allows the preparation of spectrally narrow hot-exciton distributions [2, 3]. Also, new quantum-kinetics phenomena like the coherent coupling of electron states by multiple phonons are observed [6].

We will review here some recent studies of ultrafast phenomena in ZnSe-based QWs by transient four-wave mixing (FWM) and time-resolved photoluminescence (TRPL). The former method probes the coherent polarization of the QW sample related to optical excitations (e.g. excitons and biexcitons) after generation by a short laser pulse [7]. The degree of this phase coherence is determined from the self-diffraction efficiency of a transient grating written by two pulses with k-vectors k_1 and k_2 which impinge onto the sample under a small angle. Interactions of the optical excitations like exciton–exciton or exciton–phonon scattering destroy the phase coherence. One gains information on these interactions from the evolution of the diffracted signal in direction $2k_2 - k_1$ as a function of a temporal delay between the two incident pulses.

Studies of the incoherent dynamics of excitons using TRPL reveal the mechanisms of energy relaxation after the generation of excitons with some excess energy. Again, the interactions of the excitons among themselves and with phonons lead to a thermalization and the latter process also to a cooling of the exciton distribution. The distribution function of the (non-)thermal exciton population can be deduced from time-resolved phonon-sideband spectroscopy [2, 3]. The LO phonon-assisted recombination of the excitons is here recorded by a synchroscan streak camera after generation of hot excitons using a picosecond pulse.

After a description of the samples and the experimental setup (Sec. 2), we will focus in Section 3 on the interaction of excitons with a background exciton density created by a prepulse. We determine the interaction strength and discuss the differences between scattering of coherent and incoherent excitons. Then we will describe the thermalization dynamics of hot excitons as a function of initial excess energy (Sec. 4).

2. Samples and experimental details

The investigated samples are multiple quantum wells (MQWs) with 10 periods of ZnSe/ZnMgSSe grown by molecular beam epitaxy. The composition of the quaternary barriers is such that the samples are lattice-matched to the GaAs substrate. The ZnSe wells are thus slightly strained. The thickness of the wells will be indicated where necessary. For the TRPL experiments, we used additionally a 180 periods ZnSe/ZnSSe MQW grown by metal organic vapor phase epitaxy. The ZnSe layer thickness is here 7.3 nm with a sulphur content of 10% in the barrier.

The FWM experiments were performed with 100 fs pulses from a frequency doubled Ti:sapphire laser. The spectral width of the pulses was about 20 meV and the maximum was tuned to the $1s$ hh exciton resonance. The detection of the FWM signal in $2k_2 - k_1$ direction was spectrally resolved by a spectrometer and an optical multichannel analyser. For the TRPL the laser pulses were narrowed spectrally to about 2 meV. Spectral and temporal resolutions were achieved by a combination of spectrometer, synchroscan streak camera, and optical multichannel analyser. All experiments were performed at a lattice temperature of 5 K.

3. Coherent spectroscopy of exciton–exciton interactions

A typical series of FWM spectra as a function of delay time τ_{12} between the pulses $\boldsymbol{k}_2$ and $\boldsymbol{k}_1$ is given in the contour plot of Fig. 1 for the case of 5-nm QWs. The signal is dominated by a contribution at the spectral position of the hh-exciton resonance (X_{hh}). The two weaker (and also faster decaying) features (XX and $X+X$) have a biexcitonic origin which was verified by using various configurations of the pump-pulse polarization and by observation of quantum beats. These latter contributions influence significantly the FWM signal at short delay times τ_{21}. This rather complex behavior will be discussed in more detail elsewhere [8].

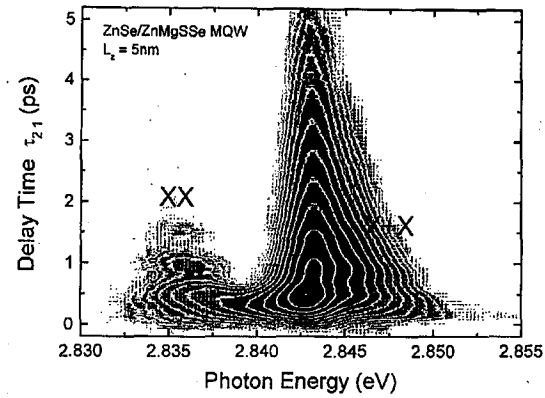

Fig. 1. FWM-signal intensity as a function of photon energy and delay time τ_{21}. The logarithmic contour plot of the intensity spans 2.5 orders of magnitude. Besides the exciton (X_{hh}), contributions from the biexciton (XX) and the biexciton continuum/anti-bound two-exciton state ($X+X$) are observed.

We will focus now onto the final decay of the coherent hh-exciton polarization. The homogeneous linewidth $\Gamma_{\mathrm{hom}} = 2\hbar/T_2$ of the hh exciton can be determined from an exponential fit to the FWM signal decay, which directly yields for an inhomogeneously broadened system $T_2/4$ (T_2 is the dephasing time). We investigated the increase in Γ_{hom} due to the interaction with a background of excitons created initially within the same volume in phase space. This background is generated by a prepulse cut from the same laser beam as the two pump pulses. It impinges onto the sample with selected (negative) delay times τ_{31}. A clear reduction of the signal decay time is evident from Fig. 2 in this case. The reason for this behavior is the density dependent mutual interaction of the excitons [9, 10].

It is also obvious that the decay-time reduction (or increase in Γ_{hom}) recovers partially when the prepulse arrives before the first pump pulse (negative τ_{31}) rather than simultaneously. This behavior is further illustrated in Fig. 3 where the homogeneous linewidth of the hh exciton is plotted as a function of prepump delay time τ_{31}. On the timescale of the dephasing of the macroscopic polarization related to the background exciton population, Γ_{hom} drops by about 30% to reach a value close to the one without prepump. We interpret this finding as a clear

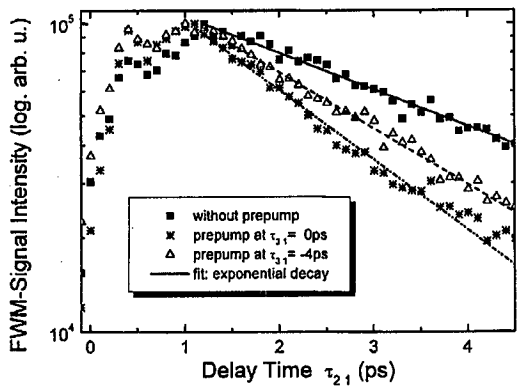

Fig. 2. Temporal evolution of the X_{hh} FWM signal for different prepump delay times and without prepump.

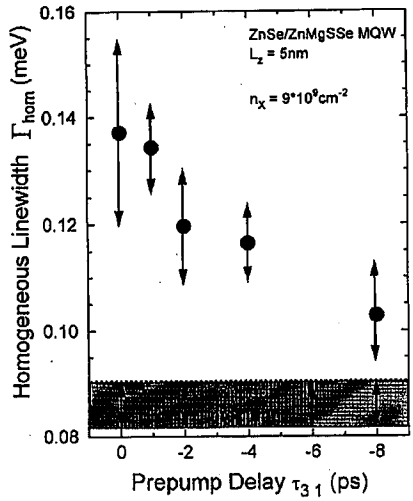

Fig. 3. Homogeneous linewidth of the hh exciton as a function of prepump delay for a fixed background exciton density n_X. The shaded area marks the typical range of Γ_{hom} when determined without prepump.

indication that the excitonic interactions are far more efficient between coherent excitons than between incoherent ones [11].

The increase in the excitonic scattering rate upon rising the exciton density is demonstrated in Fig. 4. The dephasing time, and thus Γ_{hom}, of the hh exciton change monotonously with prepulse intensity. The data in Fig. 4 are fitted with the relation $\Gamma_{\mathrm{hom}}(n_X) = \Gamma_{\mathrm{hom}}(0) + \gamma_{XX} a_{\mathrm{B}}{}^2 E_{\mathrm{B}} n_X$, where a_{B} and E_{B} are the Bohr radius and binding energy of the exciton, respectively [9, 10]. We find an exciton–exciton interaction parameter γ_{XX} of about 4 and 1.1 depending on the negative delay time of the prepump. These interaction parameters are quite similar

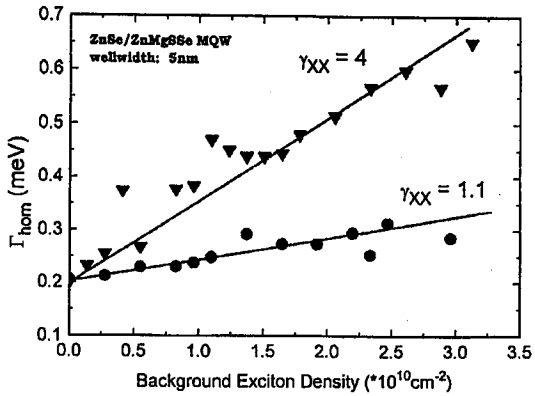

Fig. 4. Homogeneous linewidth of the hh exciton as a function of background exciton density. The triangles mark the data measured for a prepump delay $\tau_{31} = 0$ ps (coherent excitons), while the dots are recorded for $\tau_{31} = -5$ ps (incoherent excitons). The straight lines are used to determine the exciton scattering parameter γ_{XX}.

to the ones found in ZnSe/ZnSSe QWs [1], in wide ZnSe/ZnMgSe QWs [11], in CdTe/CdZnTe QWs [12], and in GaAs/AlGaAs QWs [10]. But, it is a striking result that the interaction parameter in the case of coherent exciton interaction ($\tau_{31} = 0$ ps) is nearly four times larger than the one for a dephased background population ($\tau_{31} = -5$ ps).

4. Thermalization of hot excitons

In this section we will discuss the interaction of excitons in ZnSe QWs with phonons investigated with TRPL. We use the strong Fröhlich coupling of the excitons to the LO phonons twice in these experiments. First, a spectrally narrow hot-exciton distribution is created on the $1s$ hh exciton parabola after excitation in the range of the excitonic continuum [2, 3]. Photoluminescence excitation spectroscopy reveals that this LO-phonon assisted exciton formation is the dominant relaxation mechanism in ZnSe QWs [3]. The hot excitons are usually not accessible to a PL experiment because excitons with such large momenta cannot couple to photons. But the LO-phonon sideband emission directly reflects the hot-exciton distribution in the dispersion parabola.

These relaxation and scattering processes as well as an experimental cw PL spectrum are shown in Fig. 5. The zero-phonon emission (hh) reflects only the excitons which have already relaxed towards $\boldsymbol{k} = 0$ and the excitons in localized tail states. The sideband emission, however, shows besides the phonon replica of the zero-phonon line (hh-LO) also a pronounced peak (bold arrow) resulting from the hot-exciton recombination.

The dynamics of the hot-exciton relaxation and thermalization are revealed from time-resolved phonon-sideband spectroscopy (Fig. 6). The narrow hot-exciton distribution after the LO-phonon assisted exciton generation is clearly seen in the spectra around time $t = 0$ ps. Of course, this hot-exciton feature shifts according to the photon energy of the exciting laser pulse. It is thus possible to generate a

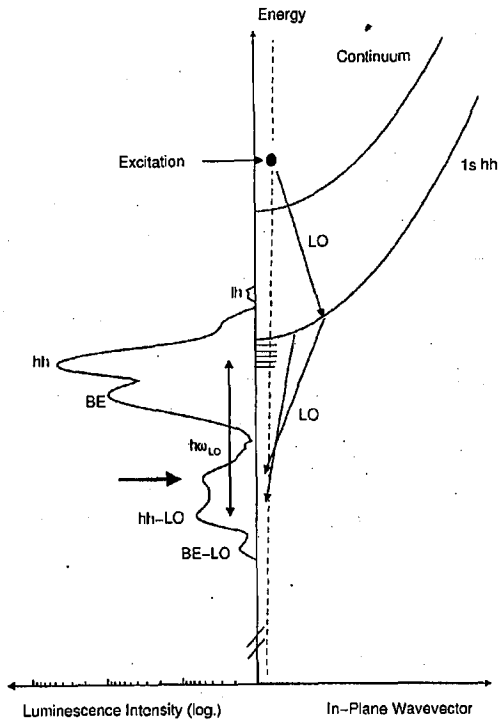

Fig. 5. Schematic depiction of excitonic relaxation in ZnSe QWs. The right side shows the $1s$ hh exciton (solid line) and photon (dashed line) dispersions as well as the dominant relaxation paths assisted by optical phonons. The left side is a photoluminescence spectrum of a ZnSe/ZnSSe MQW for a cw excitation at the energy indicated by the solid dot. The phonon sideband emission shows clear signatures of a hot-exciton population (bold arrow).

narrow hot exciton distribution on the $1s$ hh parabola with an initial excess kinetic energy of up to 20 meV. The following spectra at longer times after excitation show the gradual relaxation on the parabola by interaction with acoustic phonon mainly via the deformation-potential scattering. This scattering mechanism is rather inefficient with an average scattering time of some 10 ps. Consequently, a thermalized exciton distribution is only found after about 100 ps.

These experimental findings are in good qualitative agreement with theoretical simulations of the relaxation mechanisms (Fig. 7). The theory is based on the calculation of the exciton scattering rates from Fermi's Golden Rule [2, 13]. We treat the relaxation for free as well as for localized exciton states. Transition matrix elements are explicitly determined for deformation-potential scattering by LA phonons and piezo-electric scattering by LA and TA phonons. A rising of the initial kinetic energy results in a slowing down of the thermalization. Especially, more excitons are then lost due to nonradiative processes and do not reach the states at the minimum of the parabola at $E_{\mathrm{kin}} = 0$ and the localized tail states.

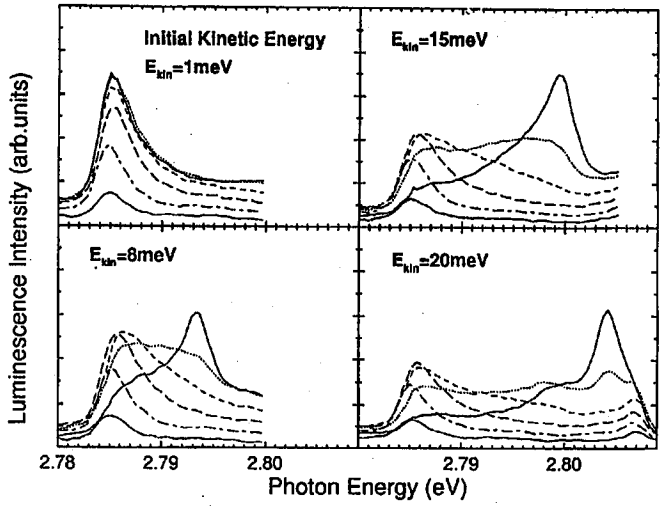

Fig. 6. Photoluminescence spectra taken at 0 ps (solid lines), 35 ps (dotted lines), 70 ps (short–dashed lines), 140 ps (long–dashed lines), 280 ps (dashed–dotted lines), and 560 ps (solid lines) after a 1 ps excitation pulse. The initial kinetic energy within the 1s hh parabola is reached after the emission of the first LO phonon (see Fig. 5).

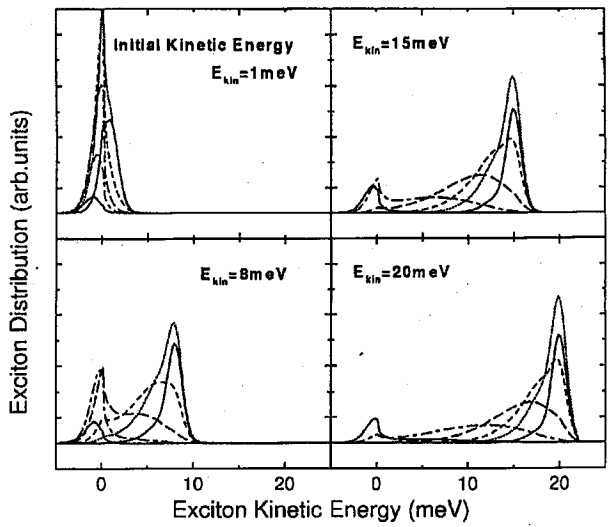

Fig. 7. Calculated exciton population in the 1*s* hh parabola for the same time delays as in Fig. 6 after LO-phonon assisted generation of a spectrally sharp hot exciton distribution for various initial kinetic energies.

The overall dynamics is found to be a factor of two faster in the experimental data as compared to the theory. This is most probably due to the approximations made in the calculations and due to the fact that the strict wave-vector conser-

vation was used for the in-plane wave vectors. Still, good qualitative agreement with experimental spectra is achieved also for the case of cw photoluminescence and photoluminescence excitation spectroscopy [3].

5. Summary

The coherent and incoherent dynamics of excitons in ZnSe quantum wells has been studied. The high exciton binding energy and the strong coupling to LO phonons allow an improvement of experimental procedures and give a better access to exciton dynamics as compared to III–V quantum wells. Especially, the mutual interaction of coherent excitons is found to be a factor of four more efficient than the one of incoherent excitons. The thermalization of hot excitons due to scattering with acoustic phonons occurs on a 100 ps timescale.

Acknowledgments

We gratefully acknowledge fruitful collaborations with M. Umlauff, W. Langbein, and J.M. Hvam, very helpful discussions with R. v. Baltz and V.M. Axt, as well as the growth of excellent samples by K. Ohkawa, B. Jobst, D. Hommel, M. Scholl, J. Söllner and M. Heuken. This work has been supported by a fund from the Deutsche Forschungsgemeinschaft within the special program on "Quantum Coherence of Semiconductors".

References

[1] H.P. Wagner, A. Schätz, R. Maier, W. Langbein, J.M. Hvam, *Phys. Rev. B* **56**, 12581 (1997).

[2] M. Umlauff, J. Hoffmann, H. Kalt, W. Langbein, J.M. Hvam, M. Scholl, J. Söllner, M. Heuken, B. Jobst, D. Hommel, *Phys. Rev. B* **57**, 1390 (1998).

[3] H. Kalt, J. Hoffmann, W. Langbein, J.M. Hvam, M. Scholl, J. Söllner, M. Heuken, B. Jobst, D. Hommel, *J. Cryst. Growth* **184/185**, 795 (1998).

[4] W. Langbein, J.M. Hvam, M. Umlauff, H. Kalt, B. Jobst, D. Hommel, *Phys. Rev. B* **55**, R7383 (1997).

[5] H. Nickolaus, F. Henneberger, *Phys. Rev. B* **57**, 8774 (1998).

[6] D. Steinbach, G. Kocherscheidt, M.U. Wehner, H. Kalt, M. Wegener, K. Ohkawa, D. Hommel, submitted to *Phys. Rev. Lett.*

[7] J. Shah, *Ultrafast Spectroscopy of Semiconductors and Semiconductor Nanostructures*, in *Springer Ser. Solid-State Sci.*, Vol. 115, Springer, Berlin 1996.

[8] H. Kalt, S. Wachter, D. Lüerßen, K. Ohkawa, D. Hommel, unpublished.

[9] G. Manzke, K. Henneberger, V. May, *Phys. Status Solidi B* **139**, 233 (1987).

[10] J. Kuhl, A. Honold, L. Schultheis, *Adv. Solid State Physics/Festkörperprobleme* **29**, 157 (1989).

[11] H.P. Wagner, A. Schätz, R. Maier, W. Langbein, J.M. Hvam, *Phys. Rev. B* **57**, 1791 (1998).

[12] E.J. Mayer, N.T. Pelekanos, J. Kuhl, N. Magnea, H. Mariette, *Phys. Rev. B* **51**, 17263 (1995).

[13] T. Takagahara, *Phys. Rev. B* **26**, 6522 (1985).